Available online at www.sciencedirect.com
ScienceDirect
Trans. Nonferrous Met. Soc. China 23(2013) 23−31
Transactions of Nonferrous Metals Society of China
www.tnmsc.cn

Effects of stress state on texture and microstructure in cold drawing-bulging of CP-Ti sheet

Hong-wei LI, Xia-lu ZHANG, Jia-yuan CHEN, Jin-shan LI

State Key Laboratory of Solidification Processing, Northwestern Polytechnical University, Xi'an 710072, China

Received 8 February 2012; accepted 14 March 2012

Abstract: Three different stress states of the combination of tensile (t) stress and compressive (c) stress, t−t, t−c and t−c−c, exist in the deformed commercially pure titanium (CP-Ti) sheet during cold drawing-bulging. The textures and microstructures in the different stress state regions were investigated by means of XRD and TEM analysis. Similar development of texture and microstructure is achieved with less thickness strain under multiaxial stresses in drawing-bulging than in cold rolling. The results show that texture and microstructure are much sensitive to multiaxial stresses. Twinning is more easily activated under compressive stress than tensile stress. Prism $\langle a \rangle$ slip is heavily affected by tensile stress, resulting in a remarkable change of the intensity of (0°, 35°, 0°) texture, while pyramidal $\langle c+a \rangle$ slip, forming (20°, 35°, 30°) texture, weakens with the increase of thickness strain in spite of stress state.

Key words: titanium alloy; texture; twinning; microstructure; drawing; stress state; cold rolling; drawing-bulging

1 Introduction

Duplicated micro-mechanism of commercially pure titanium (CP-Ti) is observed in terms of its hexagonal close packed (HCP) crystallographic structure. $\langle a \rangle$-type dislocations are easily activated and $\langle c+a \rangle$ slip or twinning is additionally activated to accommodate an external strain imposed on the grain [1]. This leads to the development of microstructure and texture, resulting in different mechanical properties of the deformed material in contrast with the as-received one. Transmission electron microscopy (TEM), X-ray diffraction (XRD) and electron back-scattered diffraction (EBSD) techniques provide powerful methods for characterizing the microstructure and texture evolution during deformation. Through these techniques, the developments of microstructure and texture of CP-Ti are investigated to answer how and why it deforms in a certain way.

The developments of texture and microstructure vary with the deformation amount. For low to medium deformation up to 40% in thickness reduction after cold rolling, the external strain is observed to be accommodated by slip and twinning but by slip dominantly for heavy deformation between 60% and 90% in thickness reduction. As a result, a refined microstructure is generated due to twinning, and a split-basal texture and shear band are gotten due to $\langle a \rangle$ combining with $\langle c+a \rangle$ slip in heavy deformation [1]. Similarly, $\{10\bar{1}1\}$ twinning is found as a key factor for effectively reducing the deformed grain size in hot compression test, and all slip systems apart from the basal slip systems are active at a low level strain, but the basal, first- and second-order pyramidal slip systems are active at a large level strain [2]. Thus, the high-angle grain boundaries form as a function of thickness strain in cold rolling associated with three different mechanisms of microstructure formation, i.e., twinning, an increase in dislocation density and the formation of substructure, and the formation of deformation-induced high-angle boundaries [3].

In addition, the texture and microstructure are sensitive to deformation conditions. Different speed

Foundation item: Project (2010CB731701) supported by the National Basic Research Program of China; Projects (50805121, 51175428) supported by the National Natural Science Foundation of China; Project (50935007) supported by the National Natural Science Foundation of China for Key Program; Project (NPU-FFR-JC20100229) supported by the Foundation for Fundamental Research of Northwestern Polytechnical University in China; Project (2011-P06) supported by the Foundation of the State Key Laboratory of Materials Processing and Die & Mould Technology, Huazhong University of Science and Technology; Project (B08040) supported by Program of Introducing Talents of Discipline to Universities ("111"), China

Corresponding author: Hong-wei LI; Tel: +86-29-88460212; E-mail: lihongwei@nwpu.edu.cn

DOI: 10.1016/S1003-6326(13)62424-3

rolling (DSR) on CP-Ti was studied by HUANG et al [4] and KIM et al [5]. They found that DSR helped to obtain basal texture, which results in an improvement of stretch formability. A large strain in equal channel angular pressing (ECAP) also causes distinct developments of texture and microstructure [6−9]. In addition, the deformation temperature is a key factor affecting the evolution of texture and microstructure [10]. LIU et al [11] studied the development of texture during a dual-temperature square-shaped deep-drawing CP-titanium sheet. They found that ND-fiber textures were intensified under dual-temperature condition, which indicates that the slip systems along ⟨*a*⟩ axis and ⟨*c*+*a*⟩ axis are both activated at a high temperature, resulting in a better drawability. Microstructure mechanism is also dependent on the initial microstructure and texture. The volume fraction and length of twins are strongly dependent on the initial grain size [12], and distinct microstructures with different microhardness after ECAP can be obtained due to the initial microstructures [8]. Moreover, the strain hardening and twin activity of CP-Ti are different for samples with different initial orientations. The samples with basal orientations undergo minimal twinning and exhibit the least hardening, while a higher yield strength due to the activation of the harder pyramidal slip system. However, they yield the same end texture under quasi-static compression despite different initial textures and microstructural evolution in terms of twin boundaries [13].

Besides the deformation conditions, the loading modes strongly affect the dominant mechanisms in the deformation of CP-Ti which control the mechanical properties [14]. Therefore, the stress state in cold drawing-bulging should do great effects on the developments of texture and microstructure of CP-Ti. Also, the texture and microstructure of CP-Ti obtained after deformation affect its mechanical performance in turn. For example, the crystallographic texture in cold rolling controls the mechanical properties anisotropy of CP-Ti, while the microstructure refining and mechanical twins have fewer significant effects [14]. Therefore, it is necessary to make it clear how the texture and microstructure evolve in order to improve the drawability during the cold drawing-bulging process and how the mechanical properties of the formed part are in order to improve the performance. It is required by ascending industrial requirements on thin-walled semispherical part of CP-Ti which is usually produced through the drawing-bulging technique.

Similar but different with the deep drawing process, the drawing-bulging process combines the characters of deep drawing process, as that in the flange zone (FZ) and drawing zone (DZ), with the bulging process, as that in the dome (called bulging zone, BZ), illustrated by segments *AB*, *CD* and *DO* in Fig. 1, respectively. Different stress states in these zones during the forming process can be easily analyzed [15]: the tensile stress in radial direction and compressive stress in the circumferential direction in DZ and FZ where the compressive stress exists in the thickness direction as well, and the tensile stress in both the radial direction and circumferential direction in BZ. Therefore, this work will present the results of the development of microstructures and textures obtained through TEM and XRD to make the effects of stress state in the drawing-bulging process clear.

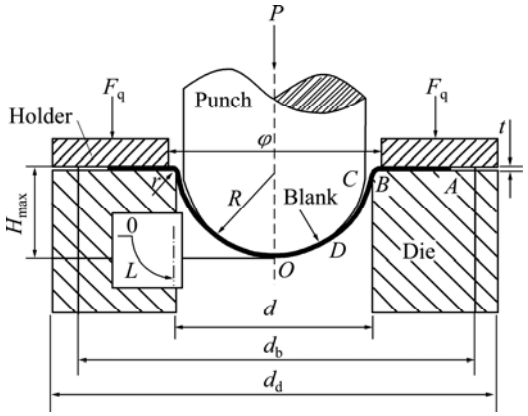

Fig.1 Scheme of cold drawing-bulging of CP-Ti sheet with illustrations of deformation zones: *AB*—FZ; *BC*—Die corner; *CD*—DZ; *DO*—BZ; *L*—thickness measurement direction

2 Experimental

The material used in this work was commercial-purity titanium, TA1, received 2-mm-thick hot-rolled and annealed plate whose measured composition is given in Table 1. The samples measuring *d*=530 mm were prepared. Configurations of the blank and tools of the drawing-bulging process are illustrated in Fig. 1 with dimensions listed in Table 2. The forming process was carried out on a 5000 kN double-action hydraulic press with the maximal stroke *H*=168 mm at room temperature. The blank was held by a rigid holder measuring *φ*=342 mm (inside diameter). The finished part is believed with a flange.

Table 1 Chemical composition of TA1 sheet

w(Ti)/%	*w*(Fe)/%	*w*(C)/%	*w*(N)/%	*w*(H)/%	*w*(O)/%
Balance	0.20	0.08	0.03	0.015	0.18

Table 2 Parameters of tools and blank

d_b/mm	d_d/mm	*d*/mm	*φ*/mm
530	630	334	348
R/mm	*r*/mm	*t*/mm	H_{max}/mm
165.5	4	1	168

Following the drawing-bulging process, the wall thickness of the finished part was measured by a PX−7 ultrasonic thickness indicator along the curved generatrix illustrated as L in Fig. 1. The mechanical properties were also tested with an INSTRON5581 tensile testing machine. Moreover, the optical microscopy (OM), XRD analysis and TEM were conducted on the specimens cut from different positions of the finished part. For the optical microscopy and XRD analysis, the specimens were mechanically polished and then electro-polished in a solution consisting of perchloric acid, methyl alcohol, and normal butanol with a volume ratio of 1:6:3 using a voltage of 30 V for 15 s at −40 °C. Subsequently, the specimens were etched with the Kroll reagent solution (V(HF):V(HNO_3):V(H_2O) was 2:4:94). The microstructures of the samples were established by OM using a Leica optical microscope and grain size was averaged using the Leica Qwin software.

To determine the substructures developed during the drawing-bulging process, the TEM analysis was performed using a JEM−200CX transmission electron microscope. The specimens for TEM were thinned to 60 μm and then twin-jet electro-polished at 30 V and −40 °C using the solution mentioned above.

To measure the textures developed during the drawing-bulging process, XRD analysis was performed using a Siemens D5000X X-ray diffractometer with Cu K_α target at 40 kV and 40 mA. The orientation distribution function (ODF) was calculated based on the obtained pole figures from XRD. From the ODFs, the complete pole figures were reconstructed.

3 Results and discussion

3.1 Microstructure of as-received material

The microstructure of the as-received material, as observed in optical microscopy, comprises single-phase, uniform equiaxed α-Ti grain structure with an average grain size of about 20 μm (Fig. 2(a)). There is no second phase observed as the precipitated phase in the microstructure. The (0002) pole figure (Fig. 2(b)) illustrates a bimodal distribution of basal poles, and the maximal intensity (5.2×random) is found at locations tilted ±35° from the ND toward the TD. The initial texture is also quantified in terms of the φ_2=0° and φ_2=30° sections of ODF (Figs. 2(c, d)). Two strong textures are found at φ_2=0°: g_1 (15°, 24°, 0°) with $f(g_1)$=12.221, and g_2 (0°, 40°, 0°) with $f(g_2)$=10.162; another strong texture at φ_2=30° is found, g_3 (15°, 35°, 30°) with the maximal intensity $f(g_3)$=10.587. As analyzed in [16], textures of g_2 and g_3 are formed during the hot rolling process, while g_1 is formed during the annealing process which is unstable in subsequent deformation. Therefore, noticeable anisotropy in mechanical properties is found

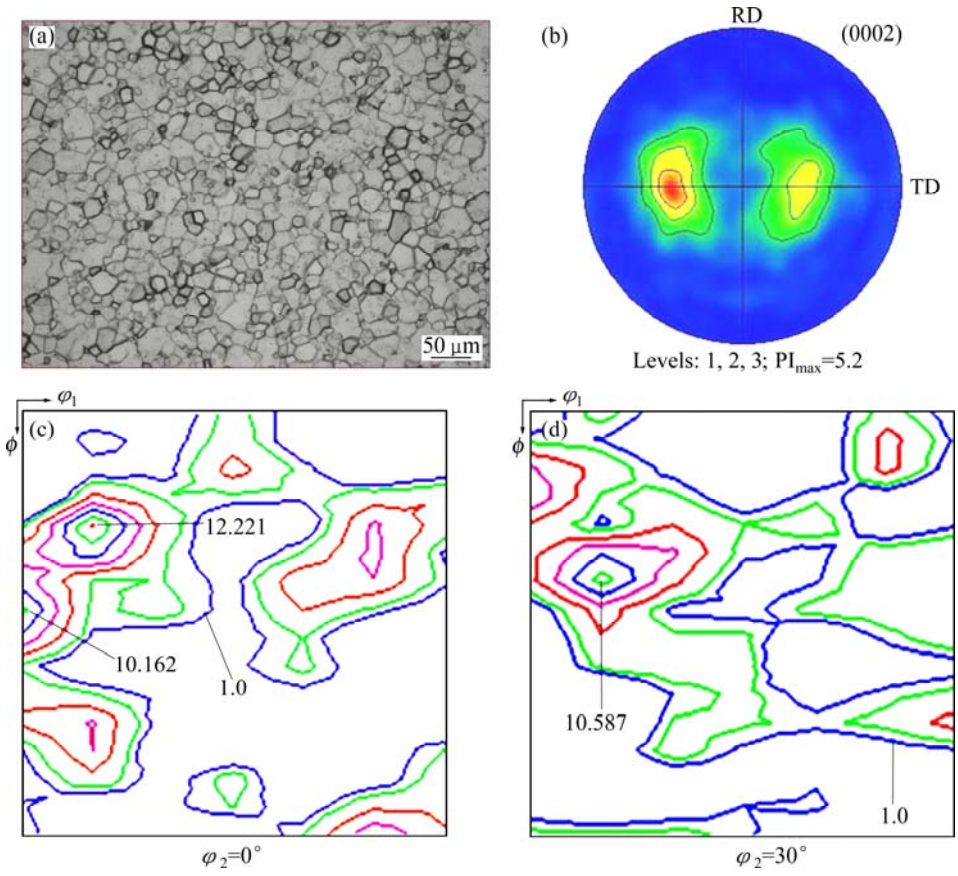

Fig. 2 Microstructure (a), (0002) pole figure (b) and ODF sections (c, d) of as-received CP-Ti sheet

as illustrated in Fig. 3(a). It shows evident differences in strength and elongation between specimens sampling in different directions (0º, 45 º and 90 º to RD).

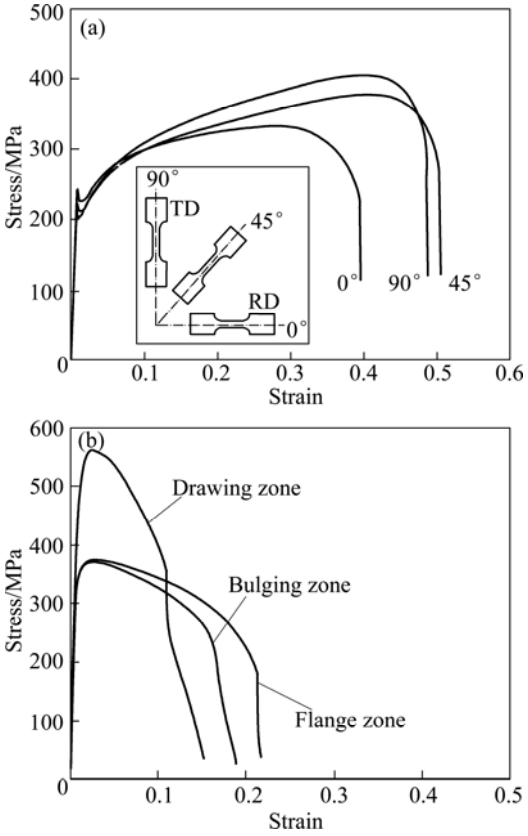

Fig. 3 Uniaxial tension test of as-received CP-Ti sheet with illustration of sampling method (a) and drawn part (b)

3.2 Non-uniform distribution of wall thickness

Essentially caused by the stress state and initial microstructure and texture, the deformation varies in each zone during the drawing-bulging process. The change of wall thickness throughout the finished part reflects the deformation. So, the wall thickness after the process is measured along the rolling direction (RD) and transverse direction (TD) of the blank, from which the change of wall thickness (wall thinning) is so calculated, as illustrated in Fig. 4. It shows remarkable difference in the distribution of wall thickness along RD and TD. The maximal wall thinning happens in DZ where the maximal deformation reaches; the minor one happens in BZ where the thickness thinning increases with increasing L, indicating the character of the bulging deformation (the tensile stress in the radial direction and circumferential direction); the minimal one happens in the flange zone (FZ). The maximal thickness strain ($\varepsilon_{thick}=\ln(t_0/t)$, where t_0 and t are the thicknesses before and after forming, respectively) calculated in different zones are 0.03 in FZ, 0.09 at H= 20 mm in DZ and 0.05 at H=160 mm in BZ. In spite of the anisotropic strain in the deformation zones, anisotropic stress responses are also found (Fig. 3(b)). Therefore, all the specimens used in this work are sampled at these three positions to reflect the effects of stress state on the evolution of texture and microstructure.

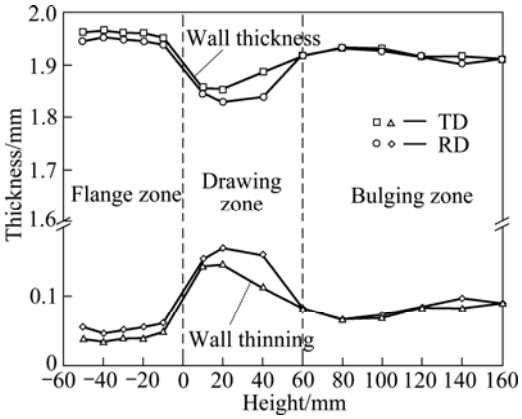

Fig. 4 Distributions of wall thickness and wall thinning (thickness reduction) of deformed semispherical part

3.3 Textures evolution in different deformation zones

The development of texture during the drawing-bulging process is quantified and interpreted in terms of φ_2=0° and φ_2=30° sections of ODF maps (Fig. 5). The annealing-induced texture g_1 (15°, 24°, 0°) of the as-received material (Fig. 2(c)) annihilates during the drawing-bulging process. This indicates the annealing-induced texture is unstable in the subsequent deformation. This is in agreement with the result in Ref. [16]. The location of the rolling-induced texture g_2 progresses from (0°, 40°, 0°) under the undeformed condition to (0°, 36°, 0°) in BZ and (0°, 48°, 0°) in DZ, while keeps unchanged in FZ of the deformed part. It was formed due to different stress states in these deformation zones. As the stress analysis, an almost stress equilibrium is obtained in BZ (equilibrium of double tensile stress in RD and CD) and FZ (equilibrium of tensile stress in CD and compressive stress in thickness direction, TD), while strong tensile stress in RD is found in DZ. Therefore, this texture rotates to RD under the dominant tensile stress in DZ. Simultaneously, the intensity of this texture increases from 10.162 in the undeformed part to 12.221 in BZ and 10.66 in DZ, while decreases to 9.336 in FZ under the deformed condition. Since this texture is formed due to prism $\langle a\rangle$ slip, it shows that predominant prism $\langle a\rangle$ slip appears in BZ and DZ, while, does not appear in FZ. Thus, the external strain in FZ is believed to be accommodated by $\{11\bar{2}2\}\langle 11\bar{2}\bar{3}\rangle$ compressive twinning and $\{10\bar{1}2\}\langle 10\bar{1}\,\bar{1}\rangle$ tensile twinning, as suggested by CHUN et al [1], which can be proved by Figs. 5(b_1, b_2). In contrast, the rolling-induced texture g_3 (20°, 35°, 30°) does not change its position but weakens with the increase of thickness strain, i.e. thickness

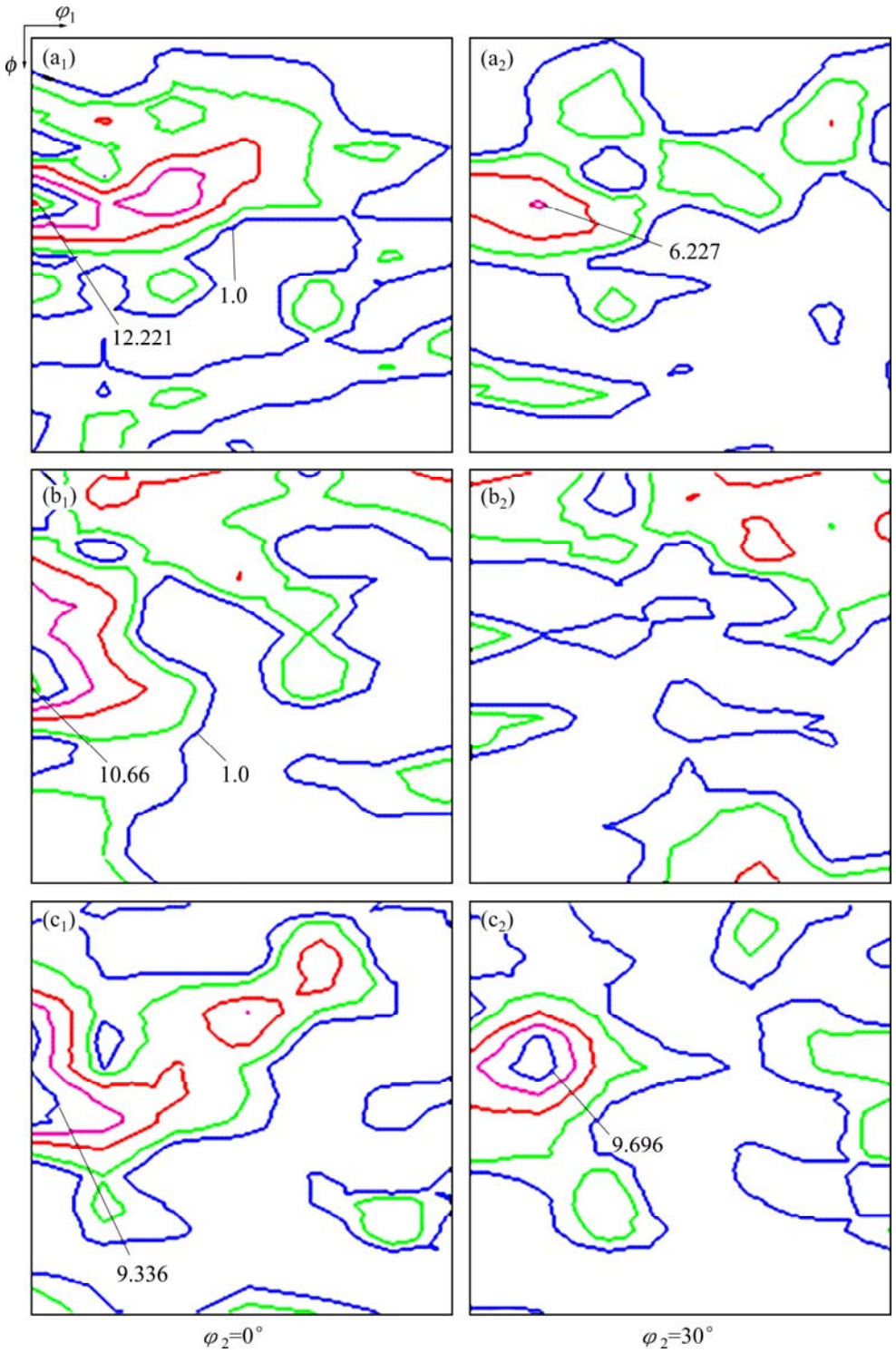

Fig. 5 ODF sections of samples in BZ (a_1, a_2), DZ (b_1, b_2) and FZ (c_1, c_2) of finished part

reduction. This texture is formed due to pyramidal ⟨*c*+*a*⟩-slip, for which the critical resolved shear stress is relatively high [1]. Therefore, twinning is activated with the increase of thickness strain. This agrees with the result achieved in cold rolling [1] except for the unchanged orientation. Interaction of the multiaxial stresses in these deformation zones cannot make any one dominant which will rotate the orientation towards the direction of itself.

3.4 Development of microstructures during drawing-bugling process

The microstructure development in different deformation zones of the finished part was firstly studied

through optical microscopy. As illustrated in Fig. 6, many grains retain equiaxed shape with clear boundaries in BZ, which is similar to the as-received material except for the formation of twins in a few grains. The dispersed low-density high-energy-state dislocations (curved shape) are observed at the triangular grain boundaries (Fig. 7(a)) and within a grain (Fig. 7(c), which shows that the external strain is accommodated mainly by slip. However, dislocation loops are observed at white arrows in Fig. 7(b) indicating the obstruction on dislocations movement. Also, a few twins are observed within a grain (Fig. 7(c)) and at grain boundaries (Fig. 7(d)), and more twins indicated by the stacking fault at the black arrow are coming [17].

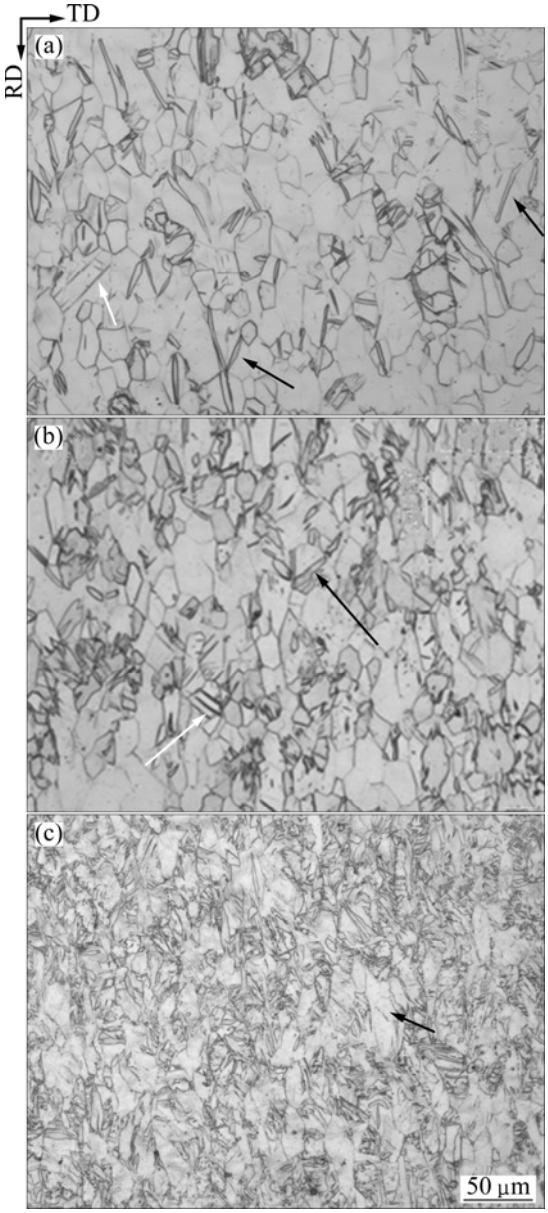

Fig. 6 Optical microscopy images of samples in BZ (a), FZ (b) and DZ (c) of finished part with illustration of large-size twins by black arrows and small-size twins by white arrows

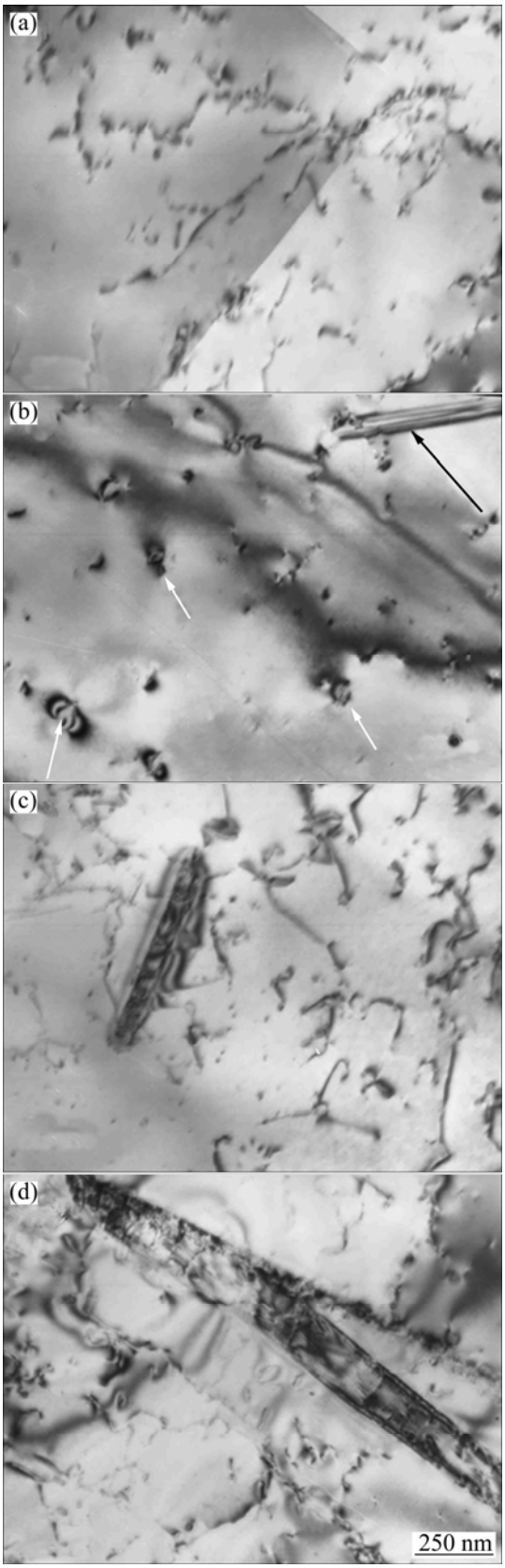

Fig. 7 TEM images in BZ: (a) Dislocations at grain boundary; (b) Dislocation loops (at white arrows) and stacking fault (at black arrow); (c) Twin and dislocations within a grain; (d) Twins at grain boundary

In FZ, similar microstructure as that in BZ can be observed. In Fig. 6(b), the grain boundaries with and without twins are clearly identified; the twins at black arrows are with large sizes, lenticular morphology and nonstraight boundaries, while small and slender twins with straight boundaries are observed at the white arrow. However, high-density dislocations at the triangular grain boundaries (Fig. 8(a)) and within a grain (Fig. 8(b)) and more twins (Figs. 8(c), (d)) are also observed. The contribution of twins on external strain is enhanced since the secondary (Fig. 8(c)) and parallel twins (Fig. 8(d)) exist. Comparison of the microstructures in these two deformation zones indicates that twinning is activated at the beginning of deformation, as suggested in Ref. [1,2]. Nevertheless, more twins are observed in FZ with a smaller thickness strain than in BZ, which is against the results in cold rolling under medium deformation [1,2]. The reason would be that twinning is more sensitive to the compressive stress, resulting in noticeable evolution of microstructure, than tensile stress.

However, a significant refinement of the microstructure is observed in DZ as shown in Fig. 6(c). Twin interactions that twin a penetrates twin b (Fig. 9(c)) and twin 1 and twin 2 are stopped by twin 3 (Fig. 9(d)), cause the refinement, so that the grain boundaries are hard to be identified (Fig. 6(c)). The interaction of twins and the dislocation cells (Fig. 9(a)) and dislocation slabs (Fig. 9(b)) results in the fragmentation of grains with about 2 μm-size lamellar structure. In contrast, a few grains remain coarse but elongated along RD, as shown by the black arrow in Fig. 6(c), which deform dominantly by slip due to their local crystallographic orientations. Similar results can be found in Ref. [1].

From the mentioned characters above, it can be found that the microstructure evolves under less thickness reduction after the drawing-bulging (8.5% for the maximal ε_{thick}=0.09) than cold rolling (40% in Ref. [1], 50% in Ref. [2]). It would be interpreted due to the interaction of multiaxial stresses in the drawing-bulging process.

4 Conclusions

1) The main textures of (0°, 35°, 0°) and (20°, 35°, 30°) and microstructures with high-energy-state dislocations form due to prism ⟨*a*⟩ slip and pyramidal ⟨*c*+ *a*⟩ slip, and dislocation cell, stacking fault, primary and second twinning, interaction of twinning and grain fragmentation are observed. The strain in each deformation zone is accommodated by a combination of prism ⟨*a*⟩ and pyramidal ⟨*c*+*a*⟩ slip due to low-level deformation, as well as the gradual formation of twinning.

2) Noticeable evolution of texture and microstructure after the cold drawing-bulging is achieved due to the multiaxial stresses. Twinning is more easily activated under the compressive stress than under the tensile stress. The tensile stress has more noticeable

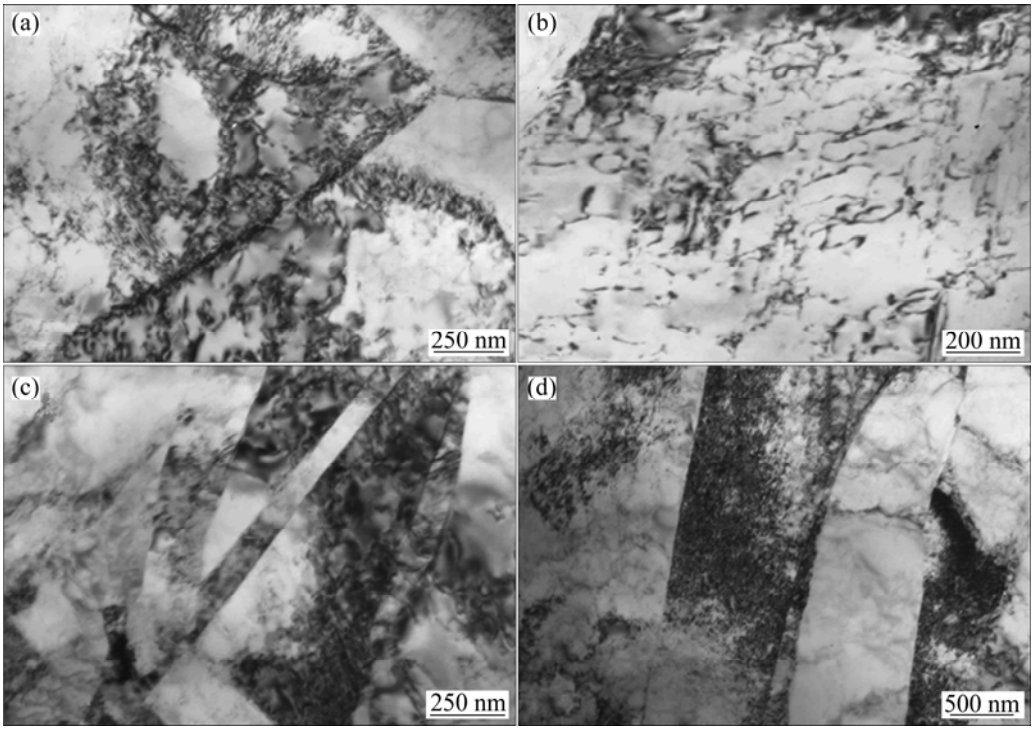

Fig. 8 TEM images in FZ: (a) Dislocations at grain boundaries; (b) Dislocations within a grain; (c) Primary and secondary twins; (d) Parallel twins

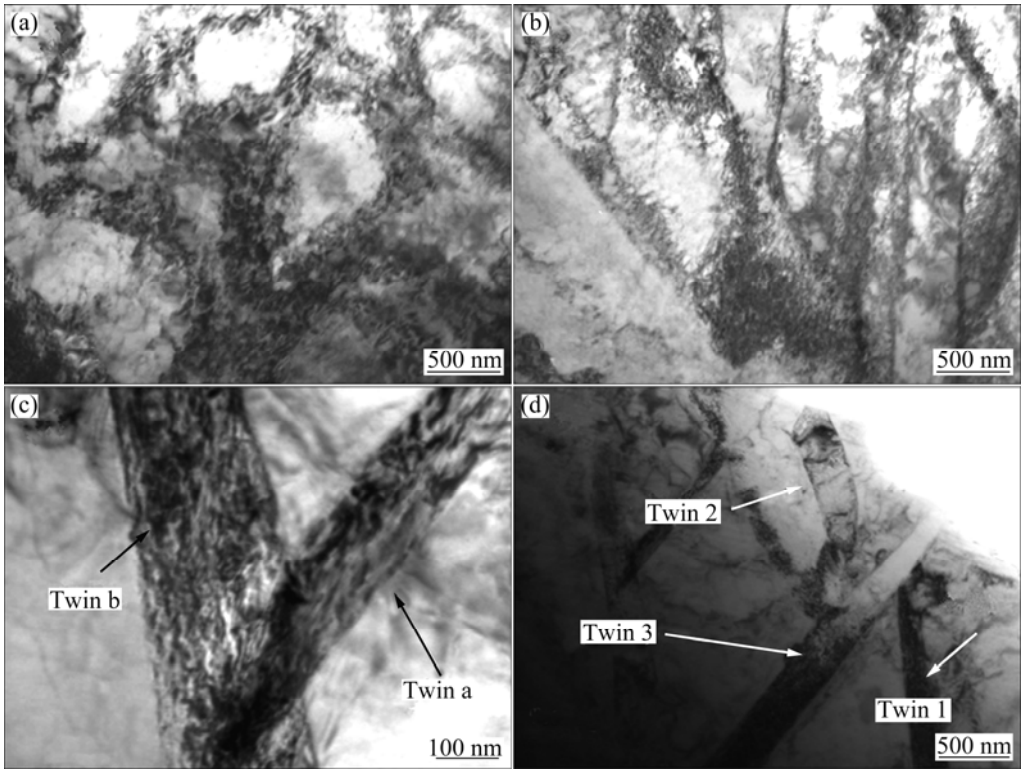

Fig. 9 TEM images in DZ: (a) Dislocation cells; (b) Slab dislocations; (c, d) Interactions of twins

effect on the prism ⟨*a*⟩ slip resulting in noticeable change in the intensity of (0°, 35°, 0°) texture, while (20°, 35°, 30°) texture owing to pyramidal ⟨*c*+*a*⟩ slip weakens with the increase of thickness strain in spite of the stress state.

References

[1] CHUN Y B, YU S H, SEMIATIN S L, HWANG S K. Effect of deformation twinning on microstructure and texture evolution during cold rolling of CP-titanium [J]. Mater Sci Eng A, 2005, 398(1−2): 209−219.

[2] ZENG Z, JONSSON S, ROVEN H J. The effects of deformation conditions on microstructure and texture of commercially pure Ti [J]. Acta Mater, 2009, 57(19): 5822−5833.

[3] ZHEREBTSOV S V, DYAKONOV G S, SALEM A A, MALYSHEVA S P, SALISHCHEV G A, SEMIATIN S L. Evolution of grain and subgrain structure during cold rolling of commercial-purity titanium [J]. Mater Sci Eng A, 2011, 528(9): 3474−3479.

[4] HUANG X, SUZUKI K, CHINO Y. Improvement of stretch formability of pure titanium sheet by differential speed rolling [J]. Scripta Mater, 2010, 63(5): 473−476.

[5] KIM W J, YOON S J, LEE J B. Microstructure and mechanical properties of pure Ti processed by high-ratio differential speed rolling at room temperature [J]. Scripta Mater, 2010, 62(7): 451−454.

[6] CHEN Y J, LI Y J, WALMSLEY J C, DUMOULIN S, SKARET P C, ROVEN H J. Microstructure evolution of commercial pure titanium during equal channel angular pressing [J]. Mater Sci Eng A, 2010, 527(3): 789−796.

[7] PURCEK G, YAPICI G G, KARAMAN I, MAIER H J. Effect of commercial purity levels on the mechanical properties of ultrafine-grained titanium [J]. Mater Sci Eng A, 2011, 528(6): 2303−2308.

[8] DHEDA S S, MOHAMED F A. Effect of initial microstructure on the processing of titanium using equal channel angular pressing [J]. Mater Sci Eng A, 2011, 528(28): 8179−8186.

[9] SUWAS S, BEAUSIR B, TÓTH L S, FUNDENBERGER J J, GOTTSTEIN G. Texture evolution in commercially pure titanium after warm equal channel angular extrusion [J]. Acta Mater, 2011, 59(3): 1121−1133.

[10] TSAO L C, WU H Y, LEONG J C, FANG C J. Flow stress behavior of commercial pure titanium sheet during warm tensile deformation [J]. Mater Des, 2012, 34: 179−184.

[11] LIU J M, CHEN I G, CHOU T S, CHOU S S. On the deformation texture of square-shaped deep-drawing commercially pure Ti sheet [J]. Mater Chem Phys, 2002, 77(3): 765−772.

[12] GHADERI A, BARNETT M R. Sensitivity of deformation twinning to grain size in titanium and magnesium [J]. Acta Mater, 2011, 59(20): 7824−7839.

[13] GURAO N P, KAPOOR R, SUWAS S. Deformation behaviour of commercially pure titanium at extreme strain rates [J]. Acta Mater, 2011, 59(9): 3431−3446.

[14] NASIRI-ABARBEKOH H, EKRAMI A, ZIAEI-MOAYYED A A, SHOHANI M. Effects of rolling reduction on mechanical properties anisotropy of commercially pure titanium [J]. Mater Des, 2012, 34: 268−274.

[15] GAO E Z, LI H W, KOU H C, CHANG H, LI J S, ZHOU L. Finite element simulation on the deep drawing of titanium thin-walled surface part [J]. Rare Metals, 2010, 29(1): 108−113.

[16] INAGAKI H. Development of cold-rolling textures in pure titanium [J]. Zeitschrift Fuer Metallkunde, 1991, 82(10): 779−789.

[17] GUO Z, MIODOWNIK A P, SAUNDERS N, SCHILLÉ J P. Influence of stacking-fault energy on high temperature creep of alpha titanium alloys [J]. Scripta Mater, 2006, 54(12): 2175−2178.

纯钛板拉胀成形中应力状态对织构和微观组织的影响

李宏伟，张下陆，陈甲元，李金山

西北工业大学 凝固技术国家重点实验室， 西安 710072

摘　要：纯钛板拉胀成形中不同部位存在 3 种不同的应力状态：拉−拉、拉−压、拉−压−压。分别在这 3 种应力状态部位取样，采用 XRD 和 TEM 方法研究这些样品的织构和微观组织。结果表明，在纯钛板冷轧过程中需要较大应变量才出现的织构和微观组织在纯钛板拉胀成形的很小厚向应变下就出现了，表明织构和微观组织对多向应力状态十分敏感；孪晶在压应力状态下比在拉应力状态下更容易激活；拉应力对棱柱型⟨*a*⟩滑移影响显著，导致(0°, 35°, 0°)织构强度明显变化；而形成(20°, 35°, 30°)织构的锥型⟨*c*+*a*⟩滑移随着厚向应变量的增加而减弱，且与受到的应力状态无关。

关键词：钛合金；织构；孪晶；微观组织；拉深；应力状态；冷轧；拉胀成形

(Edited by Hua YANG)